Copyright 2007 IEEE

Multiuser Space–Time Algorithms for Synchronization, Channel Estimation, and Data Detection in an Interference Monitoring System for UMTS/TDD Networks

Klaus Kopsa, Harold Artés, *Member, IEEE*, Gerald Matz, *Senior Member, IEEE*, and Franz Hlawatsch, *Senior Member, IEEE*

***Abstract*—We present multiuser space–time receiver algorithms for synchronization, channel estimation, and data detection in the downlink of a universal mobile telecommunications system (UMTS)/time-division duplex (TDD) cellular communication system with multiple receive antennas. These algorithms were designed for use in a network monitoring device that analyzes the interference situation present, thereby allowing the operators to improve their networks. For interference analysis, we decode the broadcast channels (BCHs) of surrounding base stations. To cope with the widely differing power levels of signals received from different base stations, we combine multiuser space–time signal processing techniques with reestimation and successive cancellation schemes. Simulation results demonstrate that our algorithms enable reliable BCH data detection even at low SINR.**

***Index Terms*—Cellular communications, channel estimation, cochannel interference, data detection, multiuser processing, space–time processing, synchronization, time-division duplex (TDD), universal mobile telecommunications system (UMTS).**

I. Introduction

In CELLULAR code-division multiple access (CDMA) systems, such as the third-generation *universal mobile telecommunications system* (UMTS) [4], operators have to carefully balance cochannel interference to serve a maximum number of users with satisfactory quality. Besides thorough network planning, monitoring of the interference situation using adequate measurement devices is necessary to optimize the network. In UMTS, widely used measurement devices are trace mobiles—common mobile terminals equipped with additional measurement software and interfaces—and scrambling code scanners. These tools are useful for large-scale measurements, but in some situations, their limited signal processing power does not allow them to resolve the interfering signals with sufficient accuracy.

Paper approved by F. Santucci, the Editor for Wireless Systems Performance of IEEE Communications Society. Manuscript received March 20, 2004; revised April 4, 2006 and December 18, 2006. This work was supported in part by the EU/IST Project ANTIUM (IST-2000-26222) and in part by the WWTF Project MOHAWI (MA 44). This work has been partly published in [1]–[3].

K. Kopsa is with Accenture, A-1010 Vienna, Austria (e-mail: Klaus.Kopsa@gmx.net).

H. Artés is with Beceem Communications Inc., Santa Clara, CA 95054 USA (e-mail: Harold.Artes@ieee.org).

G. Matz and F. Hlawatsch are with the Institute of Communications and Radio-Frequency Engineering, Vienna University of Technology, A-1040 Vienna, Austria (e-mail: gmatz@nt.tuwien.ac.at; franz.hlawatsch@nt.tuwien.ac.at).

Digital Object Identifier 10.1109/TCOMM.2007.906431

Within the European Union Project ANTIUM [5], we participated in the development of a UMTS network monitoring device that significantly outperforms conventional tools. For the time-division duplex (TDD) mode of UMTS,[1] we designed a receiver chain consisting of synchronization, channel estimation, and data detection components. This receiver performs interference classification by determining the number of base stations (BSs) contributing to the received signal, obtaining synchronization, estimating the channels corresponding to the detected BSs, decoding the broadcast channel (BCH) data, and estimating the power level for each detected BS.

In this paper, we discuss the design challenges of this receiver and describe the algorithms that we have developed for synchronization, channel estimation, and data detection, as well as their interdependencies. We address an unconventional multiuser scenario, i.e., multiple access (by multiple BSs) in the *downlink*. Usually, in cellular downlinks—apart from soft-handover situations—the mobile station processes just one BS signal, whereas here, even the weak signals of distant BSs are processed. Multiple access is normally performed in the uplink and involves only users within one cell, whereas in our downlink situation, BSs from different cells are involved. Finally, our network monitoring tool only listens, i.e., no bi-directional link to the BSs is established, and no closed-loop power control is performed.

This latter point makes the decoding task very challenging because the power levels of different BS signals are widely different (due to different path losses), and thus, extremely small signal-to-interference levels can occur. To meet this challenge, the ANTIUM design featured multiple (uncalibrated) receive antennas and offline (batch) processing of the recorded receive signals. This allowed us to apply sophisticated multiuser space–time receiver algorithms that yield satisfactory performance in spite of the adverse interference scenario.

Our choice of receiver algorithms was guided by the following considerations. A space–time rake-type receiver [7], [8] would have poor performance due to the low spreading factor of UMTS/TDD. A beamforming frontend followed by some sophisticated temporal equalizer would require a calibrated antenna array. Finally, a space–time maximum likelihood sequence

[1] See [6] for a discussion of receiver algorithms for the frequency-division duplex (FDD) mode of UMTS.

0090-6778/$25.00 © 2007 IEEE

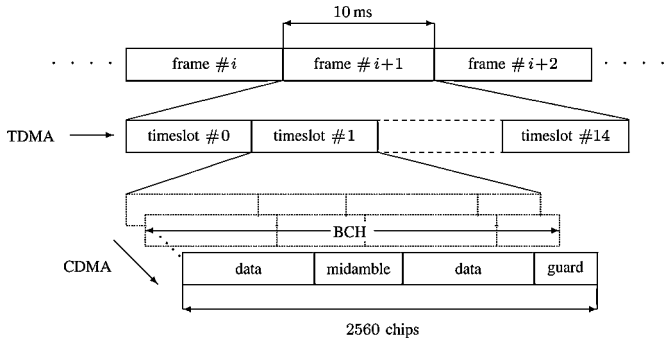

Fig. 1. Frame structure of a UMTS/TDD base station. One of the 15 timeslots of a radio frame (here, e.g., timeslot #1) contains the BCH superimposed on other CDMA channels.

estimator [9] would have excessive complexity even for offline processing. Therefore, instead of these approaches, we adopted space–time minimum mean-square error (MMSE) and decision feedback (DFB) equalizers [10]–[12] as the cores of our receiver algorithms. We embedded these equalizers in reestimation and successive cancellation schemes to compensate for the missing prior knowledge. Similar remarks apply to the synchronization and channel estimation stages preceding the MMSE/DFB detectors. A main contribution of this paper, in fact, is to demonstrate how sophisticated estimation and detection techniques have to be modified, augmented, and combined to make them work in the difficult scenario considered, under real-world conditions and without any unrealistic assumptions.

The paper is organized as follows. Section II describes synchronization algorithms for determining the number of BS signals present and the temporal location of the corresponding BCHs. In Section III, channel estimation algorithms are discussed that jointly estimate the channel impulse responses of all BSs detected by the synchronization stage. Section IV presents the data detection algorithms that equalize the channels and detect the data transmitted on the BCHs. In Section V, the performance of our algorithms is assessed through simulations. Finally, some conclusions are provided in Section VI.

II. Synchronization

We first present a brief summary of the UMTS/TDD frame structure. The frame structure of one BS is depicted in Fig. 1. With UMTS/TDD [4], all BSs are synchronized, i.e., all radio frames are transmitted temporally aligned. For a given BS, each radio frame contains 15 timeslots that can be individually allocated for uplink or downlink in a flexible manner [13]. In each timeslot, CDMA is used. One of the 15 timeslots (in Fig. 1, this is timeslot #1) contains the desired BCH and the synchronization channel (SCH) superimposed on up to 12 additional data channels. Each CDMA channel consists of two data parts separated by a midamble and followed by a guard period. The data parts are spread using a code with spreading factor 16 [14], and scrambled (modulated [14]) using a cell-specific scrambling code of length 16. The timeslot is then constituted by the sum of all CDMA channels. The antenna array of the monitoring device receives the superposition of all BS signals corrupted by frequency-selective fading and additive noise.

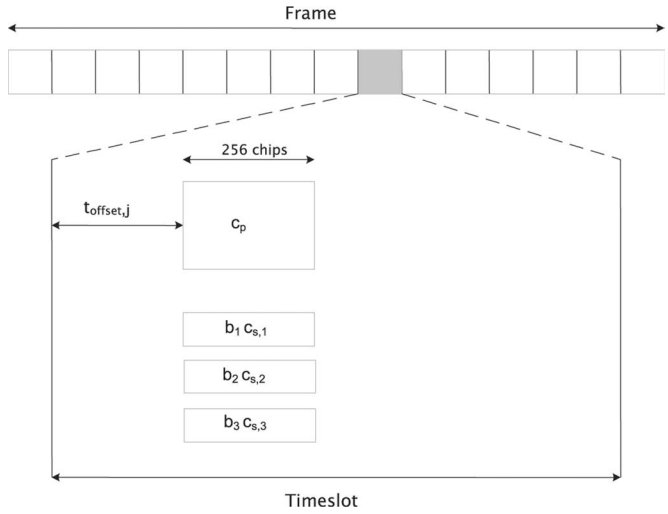

Fig. 2. Structure of the synchronization channel (SCH) [13]. The SCH is added to the data channels and the BCH present in the shaded timeslot (the data channels and BCH are not shown).

The SCH is shown in Fig. 2. It consists of a primary code sequence $c_{\mathrm{p}}(n)$ and three (out of 12 possible) secondary code sequences $c_{\mathrm{s},i}(n)$, each 256 chips long [14]. The SCH is added to the data channels and the BCH present in the respective timeslot. Because the SCHs of all BSs are transmitted in the same timeslot and the primary code sequence is identical for all BSs, each BS is assigned a different SCH time offset $t_{\mathrm{offset},j}$ to allow the receiver to distinguish (locate) the SCHs of different BSs. Each secondary synchronization code $c_{\mathrm{s},i}(n)$ is modulated with a quadrature phase-shift keying (QPSK) symbol b_i. The sum $\sum_{i=1}^{3} b_i c_{\mathrm{s},i}(n)$ is called *secondary synchronization channel*; its composition [symbols b_i and choice of the secondary code sequences $c_{\mathrm{s},i}(n)$] bears information on the BS's scrambling code, midamble, and time offset $t_{\mathrm{offset},j}$.

The synchronization procedure that we propose consists of two parts: 1) primary synchronization and 2) secondary synchronization [1], [15]. For *primary synchronization*, the peaks of a detection statistic $\gamma(n)$ indicate the locations of the primary synchronization code $c_{\mathrm{p}}(n)$. (Because $c_{\mathrm{p}}(n)$ is the same for all BSs, a single detection statistic suffices to locate the primary synchronization codes of all surrounding BSs.) Then, *secondary synchronization* performed at the obtained SCH locations yields the scrambling codes, midambles, and time offsets of the different BSs via the secondary synchronization codes. This information is used by the subsequent channel-estimation stage.

A. Primary Synchronization

We present two alternative detection statistics for primary synchronization, both of which are based on the generalized likelihood ratio test (GLRT) principle [16, p. 187]. Hereafter, $\boldsymbol{x}(n)$ denotes the $M \times 1$ baseband signal vector received on the M-element receive antenna array and sampled at the chip rate.

1) Spatial Detector: The first detector [17], [18] uses the simplifying assumption of a one-tap channel described by the single $M \times 1$ vector $\boldsymbol{h}$. Detecting the presence of the primary

synchronization code $c_{\mathrm{p}}(\cdot)$ can be formulated as the following binary hypothesis testing problem:

- $\mathcal{H}_0$ (absence of synchronization code):

$$\boldsymbol{x}(n+\nu) = \boldsymbol{w}(n+\nu), \quad \text{for } \nu = 0, \ldots, N-1.$$

- $\mathcal{H}_1$ (presence of synchronization code):

$$\boldsymbol{x}(n+\nu) = \boldsymbol{h}\, p(\nu) + \boldsymbol{w}(n+\nu), \quad \text{for } \nu = 0, \ldots, N-1.$$

Here, n is the time atwhich the two hypotheses are to be tested, $p(\nu)$ is the reference sequence (primary synchronization code $c_{\mathrm{p}}(\nu)$) of length N, and $\boldsymbol{w}(n)$ summarizes the interference from other BSs and the noise. We assume that $\boldsymbol{w}(n)$ is Gaussian and temporally white with $M \times M$ spatial correlation matrix $\boldsymbol{R}_{\boldsymbol{w}}$. Since $\boldsymbol{R}_{\boldsymbol{w}}$ and $\boldsymbol{h}$ are unknown, we have to solve a composite hypothesis testing problem. In the GLRT approach, we replace the unknown quantity $\boldsymbol{R}_{\boldsymbol{w}}$ by its conditional maximum-likelihood (ML) estimates $\hat{\boldsymbol{R}}_{\boldsymbol{w}}^{(0)}(n)$ (under $\mathcal{H}_0$) and $\hat{\boldsymbol{R}}_{\boldsymbol{w}}^{(1)}(n)$ (under $\mathcal{H}_1$) and the unknown quantity $\boldsymbol{h}$ by its ML estimate $\hat{\boldsymbol{h}}(n)$. Thus, we obtain the generalized likelihood ratio of the two hypotheses at time n as shown in (1), at the bottom of the page. The ML estimates of $\boldsymbol{R}_{\boldsymbol{w}}$ and $\boldsymbol{h}$ can be shown to be given by

$$\begin{aligned}
\hat{\boldsymbol{R}}_{\boldsymbol{w}}^{(0)}(n) &= \hat{\boldsymbol{R}}_{\boldsymbol{x}}(n) \\
\hat{\boldsymbol{R}}_{\boldsymbol{w}}^{(1)}(n) &= \hat{\boldsymbol{R}}_{\boldsymbol{x}}(n) - \frac{N}{\|p\|^2}\, \hat{\boldsymbol{r}}_{\boldsymbol{x}p}(n)\, \hat{\boldsymbol{r}}_{\boldsymbol{x}p}^H(n) \\
\hat{\boldsymbol{h}}(n) &= \frac{N}{\|p\|^2}\, \hat{\boldsymbol{r}}_{\boldsymbol{x}p}(n)
\end{aligned}$$

where $\|p\|^2 = \sum_{\nu=0}^{N-1} |p(\nu)|^2$ and

$$\hat{\boldsymbol{R}}_{\boldsymbol{x}}(n) = \frac{1}{N} \sum_{\nu=0}^{N-1} \boldsymbol{x}(n+\nu)\, \boldsymbol{x}^H(n+\nu) \tag{2}$$

$$\hat{\boldsymbol{r}}_{\boldsymbol{x}p}(n) = \frac{1}{N} \sum_{\nu=0}^{N-1} \boldsymbol{x}(n+\nu)\, p^*(\nu)\,. \tag{3}$$

The logarithm of (1), with irrelevant terms removed, then yields the detection statistic [18]

$$\gamma(n) = \frac{1}{\|p\|^2}\, \hat{\boldsymbol{r}}_{\boldsymbol{x}p}^H(n)\, \hat{\boldsymbol{R}}_{\boldsymbol{x}}^{-1}(n)\, \hat{\boldsymbol{r}}_{\boldsymbol{x}p}(n). \tag{4}$$

Since more than one frame is recorded by the ANTIUM signal acquisition unit, the performance of $\gamma(n)$ as a detection statistic can be improved through averaging over several frames.

2) Heuristic Space–Time Detector: The spatial detector (4) assumed a one-tap channel (i.e., no multipath propagation). The temporal interference caused by multipath propagation can be taken into account by stacking successive received signal vectors as $\tilde{\boldsymbol{x}}(n) \triangleq [\boldsymbol{x}^T(n)\ \ \boldsymbol{x}^T(n+1)\ \cdots\ \boldsymbol{x}^T(n+L_0-1)]^T$, where L_0 is the length of the temporal window considered. Formally substituting the ML_0-dimensional vector $\tilde{\boldsymbol{x}}(n)$ for $\boldsymbol{x}(n)$ in (4) then yields the "heuristic space–time detection statistic" (cf. [6])

$$\gamma(n) = \frac{1}{\|p\|^2}\, \hat{\boldsymbol{r}}_{\tilde{\boldsymbol{x}}p}^H(n)\, \hat{\boldsymbol{R}}_{\tilde{\boldsymbol{x}}}^{-1}(n)\, \hat{\boldsymbol{r}}_{\tilde{\boldsymbol{x}}p}(n) \tag{5}$$

where the $ML_0 \times ML_0$ matrix $\hat{\boldsymbol{R}}_{\tilde{\boldsymbol{x}}}(n)$ and the ML_0-dimensional vector $\hat{\boldsymbol{r}}_{\tilde{\boldsymbol{x}}p}(n)$ are, respectively, given by (2) and (3) with $\boldsymbol{x}(n)$ replaced by $\tilde{\boldsymbol{x}}(n)$. This detection statistic is "heuristic" as it does not correspond to a GLRT for the stacked signal vector $\tilde{\boldsymbol{x}}(n)$, but it exhibited excellent performance in our simulations (see Section V-B). Again, the performance can be further improved by averaging over several frames.

3) Choice of Threshold: A large value of the detection statistic $\gamma(n)$ in (4) or (5) indicates a high probability of presence of the code $p(\nu)$. Therefore, the result of primary synchronization is given by the "peak locations" n_i where $\gamma(n)$ exceeds a threshold η. The choice of η is a tradeoff between high detection probability and low false-alarm probability. Fig. 3 shows the (simulated) false-alarm probability versus η for the detection statistics (4) and (5) using averaging over different numbers of frames. This figure allows one to determine the threshold for a prescribed false-alarm probability. A similar approach can also be employed to determine the threshold for the GLRTs used in Sections II-B, III-B, and IV-B.

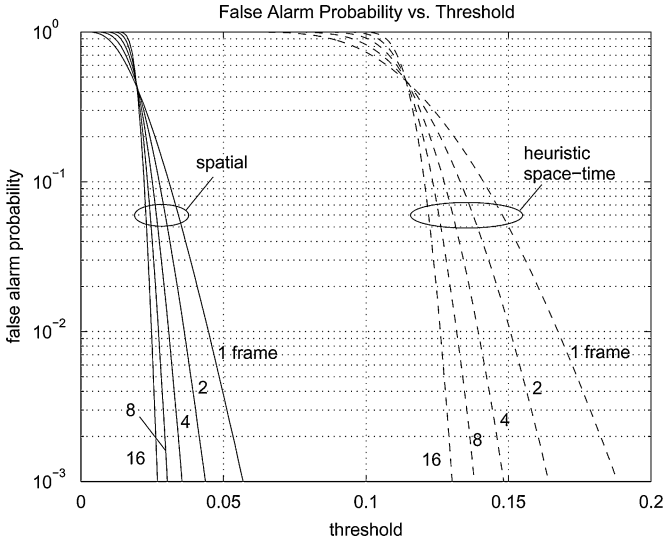

Fig. 3. False-alarm probability versus threshold η for the spatial detector and the heuristic space–time detector using averaging over different numbers of frames.

B. Secondary Synchronization

The main goal of secondary synchronization is to extract the scrambling codes, basic midambles, and time offsets $t_{\mathrm{offset},j}$ of the different BSs (this will be termed *parameter extraction* in the following). For this task, the reference sequence $p(\nu)$ in (4) or (5) is chosen as the sum of the primary synchronization code

$$L(n) = \frac{\big[\det \hat{\boldsymbol{R}}_{\boldsymbol{w}}^{(0)}(n)\big]^N \exp\big(-\sum_{\nu=0}^{N-1} \big[\boldsymbol{x}(n+\nu) - \hat{\boldsymbol{h}}(n)\, p(\nu)\big]^H \hat{\boldsymbol{R}}_{\boldsymbol{w}}^{(1)-1}(n) \big[\boldsymbol{x}(n+\nu) - \hat{\boldsymbol{h}}(n)\, p(\nu)\big]\big)}{\big[\det \hat{\boldsymbol{R}}_{\boldsymbol{w}}^{(1)}(n)\big]^N \exp\big(-\sum_{\nu=0}^{N-1} \boldsymbol{x}^H(n+\nu) \hat{\boldsymbol{R}}_{\boldsymbol{w}}^{(0)-1}(n)\, \boldsymbol{x}(n+\nu)\big)} \tag{1}$$

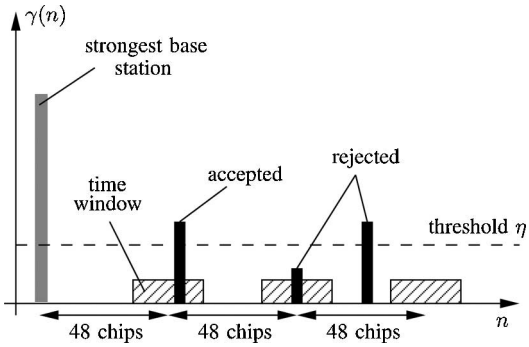

Fig. 4. Synchronization for weaker BSs using time windows.

and three weighted secondary synchronization codes, i.e.,

$$p(\nu) = c_{\mathrm{p}}(\nu) + \sum_{i=1}^{3} b_i c_{\mathrm{s},i}(\nu).$$

Since the UMTS/TDD standard allows 64 ways of composing $p(\nu)$ by choosing the b_i and $c_{\mathrm{s},i}(\nu)$, we evaluate $\gamma(n)$ at the position of the highest primary synchronization peak for all these 64 versions of $p(\nu)$. All the b_i and $c_{\mathrm{s},i}(\nu)$ corresponding to the maximum of the resulting 64 values provide the information about the BSs' basic midambles, scrambling codes, and time offsets via lookup tables specified in the standard [1], [15]. This result for the strongest BS is quite reliable since the strongest BS has a high signal-to-interference-and-noise ratio (SINR). However, because it will heavily influence the subsequent synchronization to the weaker BSs, we verify its correctness in a *synchronization verification* stage that attempts to discriminate between an actual SCH location and a false alarm [1], [15]. We use the extracted BCH midamble of the strongest BS as the reference sequence $p(\nu)$ and check whether the peak of the spatial detection statistic (4) at the position to be tested is above a certain threshold. In the negative case, we repeat parameter extraction and synchronization verification at the position of the second strongest peak in the primary synchronization detection statistic.

For secondary synchronization to the weaker BSs, we exploit the fact that the timeslots of all BS signals are temporally aligned upon transmission. The 32 possible synchronization code offsets $t_{\mathrm{offset},j}$ differ by multiples of 48 chips. Since adjacent BSs use different time offsets, we know where to expect the synchronization codes of weaker BSs. To allow for path-length depending time delays, we search for these codes in a certain time window around the expected locations, as shown in Fig. 4. Thus, for synchronization to a weaker BS, we accept a peak of $\gamma(n)$ if and only if it *both* exceeds our threshold and is located within one of the time windows (see Fig. 4). At each accepted peak location, we then perform parameter extraction and synchronization verification as described earlier for the strongest BS.

Fig. 5 summarizes the steps of the total synchronization procedure [1], [15]. The upper part describes the synchronization for the strongest BS, while the lower part describes the scanning of the 32 different time windows for the SCHs of weaker BSs.

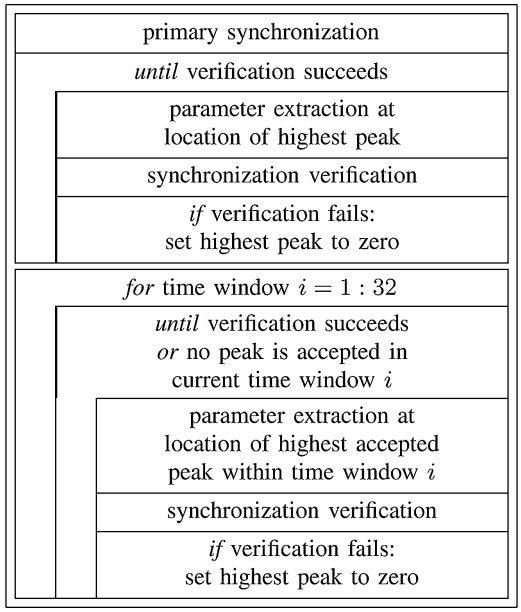

Fig. 5. Structure chart of the synchronization procedure.

III. Channel Estimation

Channel estimation is based on the midamble contained in each UMTS/TDD timeslot (cf. Fig. 1). After the synchronization stage, we know the temporal locations of the timeslots (and, thus, of the midambles) and which basic midamble sequence is used by a given BS. Because the BCHs of all BSs are transmitted in the same timeslot and the UMTS/TDD network is synchronized, the corresponding midambles are roughly temporally aligned at the receiver (only "roughly" because of the different propagation delays). Therefore, channel estimation can be performed for all BSs jointly. On the other hand, for simplicity, we estimate the channels corresponding to the individual antennas separately. This is optimum if these channels are uncorrelated, and it was observed to work well even if they are correlated.

Let K be the number of BSs detected by the synchronization stage, and L the maximum length of all channel impulse responses including propagation delays. We stack all data received on the ith antenna during the midamble period into the vector $\boldsymbol{x}_i$ of length $N_m + L - 1$ ($N_m = 512$ is the midamble length). The multiuser (i.e., containing the channels of all K BSs) input–output relation then reads [2], [15]

$$\boldsymbol{x}_i = \boldsymbol{C}\boldsymbol{h}_i + \boldsymbol{n}_i.$$

Here, the $KL \times 1$ channel vector $\boldsymbol{h}_i$ corresponds to the ith antenna; it is defined by stacking the unknown L-tap channel impulse responses of all the K BSs, and assumed Gaussian. Furthermore, the $(N_m + L - 1) \times KL$ matrix $\boldsymbol{C}$ is constructed as a row of K Toeplitz matrix blocks corresponding to the various BSs. More specifically, each one of the L columns of the kth matrix block is a delayed (shifted) replica of the midamble of the kth BS, padded by zero entries. This structure of $\boldsymbol{C}$ accounts for both the different propagation delays and the channel dispersion. Finally, $\boldsymbol{n}_i$ is a white Gaussian noise vector. The minimum mean-square error (MMSE) estimate of $\boldsymbol{h}_i$ is then given by

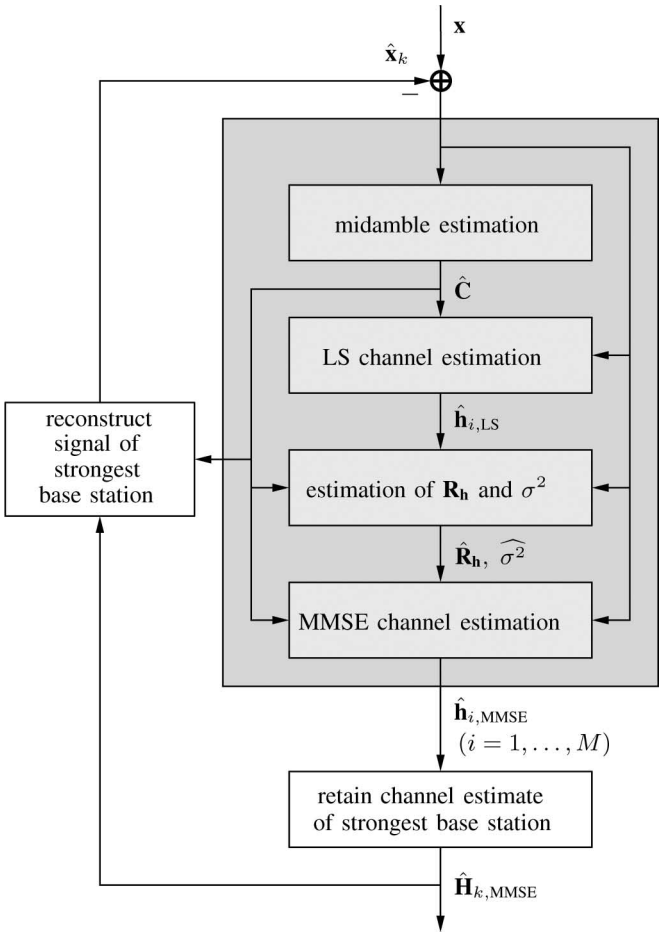

Fig. 6. Block diagram of the SC-MMSE channel estimator incorporating the MMSE channel estimator (shaded box). The index of the (currently) strongest BS is denoted by k.

[19, p. 389], [20, p. 327]

$$\hat{\boldsymbol{h}}_{i,\mathrm{MMSE}} = \boldsymbol{R_h} \boldsymbol{C}^H (\boldsymbol{C} \boldsymbol{R_h} \boldsymbol{C}^H + \sigma^2 \boldsymbol{I})^{-1} \boldsymbol{x}_i \qquad (6)$$

where $\boldsymbol{R_h}$ is the covariance matrix of $\boldsymbol{h}_i$ (assumed not to depend on i) and σ^2 is the noise variance.

A. SC-MMSE Estimator

The second-order channel statistics $\boldsymbol{R_h}$ and σ^2 (and also $\boldsymbol{C}$, cf. Section III-B) are unknown and have to be estimated. Because $\boldsymbol{h}_i$ may contain the channel impulse responses of many BSs with widely different power levels, accurate estimation of $\boldsymbol{R_h}$ is crucial. To meet this requirement, we propose to embed the MMSE channel estimator in a successive cancellation (SC) loop. The resulting *SC-MMSE channel estimator* [2], [15] is depicted in Fig. 6, with its core, the MMSE estimator, highlighted by a shaded box.

1) MMSE Estimator: The MMSE estimator consists of four stages (see Fig. 6). First, an estimate $\hat{\boldsymbol{C}}$ of the midamble matrix $\boldsymbol{C}$ is calculated as will be explained in Section III-B. Second, preliminary least-squares (LS) channel estimates [19, p. 225], [20, p. 365] $\hat{\boldsymbol{h}}_{i,\mathrm{LS}} = (\hat{\boldsymbol{C}}^H \hat{\boldsymbol{C}})^{-1} \hat{\boldsymbol{C}}^H \boldsymbol{x}_i$ are computed for several successive frames. These are used in the third step to estimate the channel statistics. Under the uncorrelated scattering assumption [21], the elements of $\boldsymbol{h}_i$ (channel taps) are uncorrelated. Thus, an estimate of $\boldsymbol{R_h}$ is given by $\hat{\boldsymbol{R}}_\boldsymbol{h} = \mathrm{diag}\{\widehat{\sigma_h^2}(1), \ldots, \widehat{\sigma_h^2}(KL)\}$, where $\widehat{\sigma_h^2}(j)$ is the sample variance of the jth element of $\hat{\boldsymbol{h}}_{i,\mathrm{LS}}$ that is computed by averaging over all antenna elements and several successive frames. Furthermore, an estimate $\widehat{\sigma^2}$ of the noise variance σ^2 is obtained as the sample variance computed from the noise vector estimate $\hat{\boldsymbol{n}}_i = \boldsymbol{x}_i - \hat{\boldsymbol{C}} \hat{\boldsymbol{h}}_{i,\mathrm{LS}}$, again using averaging over all antenna elements and several successive frames. In the fourth stage, joint MMSE estimation of the channels of all BSs previously detected by the synchronization procedure is finally performed by using the estimates $\hat{\boldsymbol{R}}_\boldsymbol{h}$ and $\widehat{\sigma^2}$ in (6).

2) Successive Interference Cancellation: The successive interference cancellation loop (see Fig. 6) attempts to prevent the signals of strong BSs from impairing the estimation of midambles and channel statistics for weaker BSs [2], [15]. In the first round, we jointly estimate the channels of all K BSs detected by the synchronization stage but retain the channel estimate of only the strongest BS. We then cancel the influence of the strongest BS by subtracting its reconstructed midamble signal from the received signal, i.e., $\boldsymbol{x} \rightarrow \boldsymbol{x} - \hat{\boldsymbol{x}}_k$ (see Fig. 6), where $\hat{\boldsymbol{x}}_k$ is the estimated midamble (cf. Section III-B) filtered by the estimated channel. This enhances the SINR of the weaker BSs so that in the second round, the midambles and channel statistics for the remaining BSs are estimated more accurately. We again retain the channel estimate of only the (currently) strongest BS and cancel the influence of this BS from the received signal. This recursive procedure continues until all channel impulse responses have been estimated.

B. Estimation of Midamble Composition

It remains to discuss the calculation of the midamble matrix estimate $\hat{\boldsymbol{C}}$ used in the LS and MMSE channel estimators. There are eight midambles $m_k^{(l)}(n)$, $l \in \{1, \ldots, 8\}$ per BS k [13], which are constructed from a cell-specific basic midamble code that is known from the synchronization stage. The BCH always uses $m_k^{(1)}(n)$, and each data channel uses one of the six midambles $m_k^{(3)}(n), \ldots, m_k^{(8)}(n)$ (up to two data channels share one midamble sequence). The midamble $m_k^{(2)}(n)$ is reserved for transmit diversity, which will not be considered here. The "total midamble" transmitted by the kth BS is thus given by a weighted superposition of the BCH midamble $m_k^{(1)}(n)$ and certain data channel midambles, i.e.,

$$m_k(n) = a_{\mathrm{ref}}\, m_k^{(1)}(n) + \sum_{l \in \mathcal{M}_k} a_k^{(l)} m_k^{(l)}(n). \qquad (7)$$

Here, the index set $\mathcal{M}_k \subseteq \{3, \ldots, 8\}$ specifies the data channel midambles, a_{ref} is the known amplitude of the BCH midamble $m_k^{(1)}(n)$ (the BCH midamble follows from the basic midamble detected during secondary synchronization; cf. Section II-B), and the $a_k^{(l)}$ are the amplitudes of the data channel midambles (which are unknown because they are affected by power control).

Channel estimation should use the total midambles $m_k(n)$ in (7) because if only the BCH midamble $m_k^{(1)}(n)$ is used, the data channel midambles will act as interferers. Hence, prior to channel estimation, we have to estimate the index sets $\mathcal{M}_k$ and the midamble amplitudes $a_k^{(l)}$ [2], [15]. With the estimates $\hat{\mathcal{M}}_k$ and $\hat{a}_k^{(l)}$, we can finally compute $\hat{\boldsymbol{C}}$ via (7). We next describe methods for calculating $\hat{\mathcal{M}}_k$ and $\hat{a}_k^{(l)}$.

1) Detection of the Index Set $\mathcal{M}_k$: A detection statistic for detecting the presence of $m_k^{(l)}(n)$ is given by the spatial detector (4) with $m_k^{(l)}(n)$ used as the reference sequence $p(n)$

$$\gamma_k^{(l)} = \frac{1}{\left\|m_k^{(l)}\right\|^2}\, \hat{\boldsymbol{r}}^H_{\boldsymbol{x}m_k^{(l)}}\, \hat{\boldsymbol{R}}_{\boldsymbol{x}}^{-1}\, \hat{\boldsymbol{r}}_{\boldsymbol{x}m_k^{(l)}}, \qquad l = 3, \ldots, 8. \quad (8)$$

We then define $\hat{\mathcal{M}}_k$ as the set of indices l for which $\gamma_k^{(l)}$ exceeds a given threshold.

2) Amplitude Estimation: For amplitude estimation, we propose a maximum-likelihood (ML) technique. We can decompose the M-dimensional received signal vector as

$$\boldsymbol{x}(n) = \boldsymbol{H}_k \boldsymbol{m}_k(n) a_{\mathrm{ref}} + \boldsymbol{H}_k \boldsymbol{M}_k(n) \boldsymbol{a}_k + \boldsymbol{w}_k(n)$$

where $\boldsymbol{H}_k$ is the $M \times L$ channel impulse response matrix of the kth BS, $\boldsymbol{m}_k(n) \stackrel{\triangle}{=} \left[m_k^{(1)}(n)\ m_k^{(1)}(n-1) \cdots m_k^{(1)}(n-L+1)\right]^T$ is the BCH midamble vector, $\boldsymbol{M}_k(n)$ is the $L \times 6$ matrix whose columns are the six data channel midamble vectors, $\boldsymbol{a}_k$ is the six-dimensional vector of the midamble amplitudes $a_k^{(l)}$, and $\boldsymbol{w}_k(n)$ summarizes all interference and noise. The ML estimator for the amplitudes $\boldsymbol{a}_k$ presupposes the knowledge of $\boldsymbol{H}_k$ and $\boldsymbol{R}_{\boldsymbol{w}}$, which is unavailable prior to channel estimation. To break this deadlock, we first calculate an *intermediate* channel estimate $\hat{\boldsymbol{H}}_k$ using a preliminary amplitude estimator. Temporarily assuming a one-tap channel vector $\boldsymbol{h}_k$, orthogonal midamble sequences $m_k^{(l)}(n)$, and no noise, (8) simplifies as $\gamma_k^{(l)} = a_k^{(l)2} \boldsymbol{h}_k^H \hat{\boldsymbol{R}}_{\boldsymbol{x}}^{-1} \boldsymbol{h}_k$. Since the BCH midamble uses the known reference amplitude a_{ref}, we also have $\gamma_k^{(1)} = a_{\mathrm{ref}}^2\, \boldsymbol{h}_k^H \hat{\boldsymbol{R}}_{\boldsymbol{x}}^{-1} \boldsymbol{h}_k$. Hence, $\gamma_k^{(l)}/\gamma_k^{(1)} = a_k^{(l)2}/a_{\mathrm{ref}}^2$, and a preliminary estimate of $a_k^{(l)}$ is given by

$$\hat{a}_{k,\mathrm{prel}}^{(l)} = a_{\mathrm{ref}} \sqrt{\frac{\gamma_k^{(l)}}{\gamma_k^{(1)}}}\,.$$

With the estimates $\hat{a}_{k,\mathrm{prel}}^{(l)}$ and $\hat{\mathcal{M}}_k$, we now calculate intermediate channel estimates $\hat{\boldsymbol{H}}_k$ by means of the SC-MMSE channel estimator. The $\hat{\boldsymbol{H}}_k$, together with estimates $\hat{\boldsymbol{R}}_{\boldsymbol{w}_k}$ of the interference/noise covariance matrices $\boldsymbol{R}_{\boldsymbol{w}_k}$ (obtained from the interference/noise estimates $\hat{\boldsymbol{w}}_k(n) = \boldsymbol{x}(n) - \hat{\boldsymbol{H}}_k \boldsymbol{m}_k(n) a_{\mathrm{ref}} - \hat{\boldsymbol{H}}_k \boldsymbol{M}_k(n) \hat{\boldsymbol{a}}_{k,\mathrm{prel}}$), are then used as prior knowledge for the ML amplitude estimator. Assuming that $\boldsymbol{w}_k(n)$ is Gaussian and temporally white, the ML estimate of $\boldsymbol{a}_k$ is obtained as [19, p. 186], [20, p. 238]

$$\hat{\boldsymbol{a}}_{k,\mathrm{ML}} = \left[\sum_{n=0}^{N-1} \boldsymbol{F}_k^H(n)\, \hat{\boldsymbol{R}}_{\boldsymbol{w}_k}^{-1}\, \boldsymbol{F}_k(n)\right]^{-1} \sum_{n=0}^{N-1} \boldsymbol{F}_k^H(n)\, \hat{\boldsymbol{R}}_{\boldsymbol{w}_k}^{-1}\, \boldsymbol{y}_k(n)$$

with the $M \times 6$ matrix $\boldsymbol{F}_k(n) \stackrel{\triangle}{=} \hat{\boldsymbol{H}}_k \boldsymbol{M}_k(n)$ and the vector $\boldsymbol{y}_k(n) \stackrel{\triangle}{=} \boldsymbol{x}(n) - \hat{\boldsymbol{H}}_k \boldsymbol{m}_k(n) a_{\mathrm{ref}}$.

IV. Data Detection

The BCH data carry most of the information required for interference monitoring [4]. After synchronization and channel estimation, all prior knowledge required to detect the BCH data of the K BSs is available. We will now present a space–time detection algorithm that uses decision-feedback equalization and successive cancellation to mitigate the effects of cochannel interference [3], [15].

A. SC-DFB Detector

1) MMSE Equalization: Stacking the BCH timeslots received on all antenna elements into the vector $\boldsymbol{x}$ of length $M(UQ + L - 1)$, where $U = 122$ is the number of symbols per timeslot (without the midamble) and $Q = 16$ is the spreading factor, we can formulate the multiuser (all K BSs) input–output relation as

$$\boldsymbol{x} = \boldsymbol{G}\boldsymbol{A}\boldsymbol{d} + \boldsymbol{n}. \quad (9)$$

Here, the $13 \cdot UK$-dimensional vector $\boldsymbol{d} = [\boldsymbol{d}_{\mathrm{BCH}}^T\ \ \boldsymbol{d}_{\mathrm{DCH}}^T]^T$ contains the symbols of all BCHs and data channels of the K BSs detected by the synchronization stage (recall that there are one BCH and up to 12 data channels per BS, hence the factor 13); $\boldsymbol{G} = [\boldsymbol{G}_{\mathrm{BCH}}\ \ \boldsymbol{G}_{\mathrm{DCH}}]$ is the total channel matrix of size $M(UQ + L - 1) \times 13 \cdot UK$ that consists of the channel impulse responses of the BSs convolved with the product of the corresponding spreading and scrambling codes; the diagonal matrix $\boldsymbol{A}$ of size $13 \cdot UK \times 13 \cdot UK$ contains the known reference amplitude of the BCHs (we normalize $\boldsymbol{A}$ such that the corresponding entries are equal to 1) and the unknown amplitudes of the data channels; and $\boldsymbol{n}$ summarizes the interference from BSs not detected by the synchronization stage and the noise.

Adopting a space–time MMSE equalization approach (e.g., [10], [20]), we obtain the detected BCH data vector as

$$\hat{\boldsymbol{d}}_{\mathrm{BCH}} = \mathrm{Q}\{\boldsymbol{F}_{\mathrm{MMSE}}\, \boldsymbol{x}\}. \quad (10)$$

Here, $\mathrm{Q}\{\cdot\}$ denotes componentwise quantization according to the QPSK symbol alphabet, and $\boldsymbol{F}_{\mathrm{MMSE}}$ is the $13 \cdot UK \times M(UQ + L - 1)$ MMSE equalizer matrix given by $\boldsymbol{F}_{\mathrm{MMSE}} = \boldsymbol{G}_{\mathrm{BCH}}^H \boldsymbol{R}_{\boldsymbol{x}}^{-1}$ (cf. (9); note that the BCH part of $\boldsymbol{A}$ does not appear because it is equal to $\boldsymbol{I}$ due to normalization). Assuming the elements of $\boldsymbol{d}$ to be uncorrelated with variance 1, we have $\boldsymbol{R}_{\boldsymbol{x}} = \boldsymbol{G}\boldsymbol{A}\boldsymbol{A}^H\boldsymbol{G}^H + \sigma_n^2 \boldsymbol{I}$.

2) Successive Interference Cancellation: The data correlation matrix $\boldsymbol{R}_{\boldsymbol{x}}$ is unknown. In Section IV-B, we will propose a structured estimator of $\boldsymbol{R}_{\boldsymbol{x}}$. Since this estimator works best for the strongest BS, we embed the MMSE detector in a successive cancellation loop. The resulting *SC-DFB detector* [3], [15] is shown in Fig. 7. After calculating $\boldsymbol{R}_{\boldsymbol{x}}$ for the strongest BS, the data of this BS are obtained by a DFB version of the MMSE detector (10) to be discussed in Section IV-C. (Although we are ultimately interested in the BCH data only, we also need

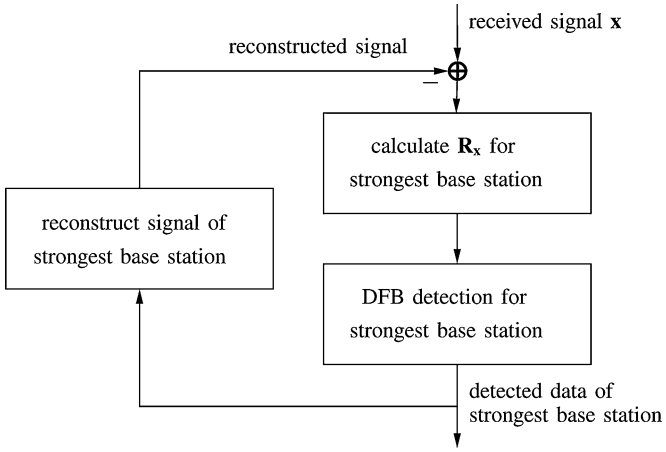

Fig. 7. Block diagram of the SC-DFB detector.

to detect the symbols of all data channels for the subsequent cancellation step.) Next, the reconstructed signal of the strongest BS is subtracted from the received signal so that the SINR for the weaker BSs is improved. Thus, in the second round, the correlation matrix of the cleaned version of $\boldsymbol{x}$ can be calculated more accurately, and better detection performance is obtained. This recursive process is continued until the data of all BSs have been detected.

For the first round, we rewrite the received signal in (9) as

$$\boldsymbol{x} = \sum_{l=1}^{K} \boldsymbol{G}_l \boldsymbol{A}_l \boldsymbol{d}_l + \boldsymbol{n} = \boldsymbol{G}_k \boldsymbol{A}_k \boldsymbol{d}_k + \boldsymbol{w}_k. \tag{11}$$

Here, k denotes the index of the strongest BS. Furthermore, the $M(UQ+L-1) \times 13 \cdot U$ matrix $\boldsymbol{G}_k$, the $13 \cdot U \times 13 \cdot U$ matrix $\boldsymbol{A}_k$, and the $13 \cdot U$-dimensional vector $\boldsymbol{d}_k$ contain the entries of $\boldsymbol{G}$, $\boldsymbol{A}$, and $\boldsymbol{d}$ corresponding to the BCH and data channels of BS k. Finally, $\boldsymbol{w}_k = \sum_{l \neq k} \boldsymbol{G}_l \boldsymbol{A}_l \boldsymbol{d}_l + \boldsymbol{n}$ summarizes the interference from all other BSs and the noise. The elements of $\boldsymbol{w}_k$ are assumed uncorrelated. With (11), the MMSE detector for the data of the strongest BS $\boldsymbol{d}_k$ is obtained as

$$\hat{\boldsymbol{d}}_k = \mathrm{Q}\{\boldsymbol{F}_{k,\mathrm{MMSE}}\, \boldsymbol{x}\}, \quad \text{with } \boldsymbol{F}_{k,\mathrm{MMSE}} = \boldsymbol{A}_k^H \boldsymbol{G}_k^H \boldsymbol{R}_{\boldsymbol{x}}^{-1} \tag{12}$$

where $\boldsymbol{F}_{k,\mathrm{MMSE}}$ is a matrix of size $13 \cdot U \times M(UQ+L-1)$, and $\boldsymbol{R}_{\boldsymbol{x}}$ is now expressed by

$$\boldsymbol{R}_{\boldsymbol{x}} = \boldsymbol{G}_k \boldsymbol{A}_k \boldsymbol{A}_k^H \boldsymbol{G}_k^H + \sigma_{\boldsymbol{w}_k}^2 \boldsymbol{I}. \tag{13}$$

B. Structured Estimation of $\boldsymbol{R}_{\boldsymbol{x}}$

Direct sample-mean estimation of $\boldsymbol{R}_{\boldsymbol{x}}$ is inaccurate due to the insufficient number of frames available for averaging. Therefore, we propose to estimate $\boldsymbol{R}_{\boldsymbol{x}}$ by exploiting the structure in (13), based on suitable estimates of $\boldsymbol{G}_k$, $\boldsymbol{A}_k$, and $\sigma_{\boldsymbol{w}_k}^2$ (as before, k is the index of the strongest BS) [3], [15]. A rough estimate of $\sigma_{\boldsymbol{w}_k}^2$ can be obtained from the quantities computed during channel estimation. Unfortunately, estimates of $\boldsymbol{G}_k$ and $\boldsymbol{A}_k$ cannot be similarly derived from the midamble set and amplitudes calculated during channel estimation (see Section III-B) because two different data channels may share one midamble sequence.

1) Estimation of $\boldsymbol{G}_k$: As mentioned earlier, $\boldsymbol{G}_k$ consists of contributions due to the BCH and the data channels of BS k; these contributions are given by the channel impulse response of BS k convolved with the product of the scrambling code and the respective spreading code. The scrambling code and channel impulse response are known from the synchronization and channel estimation stages. To determine $\boldsymbol{G}_k$, it thus remains to detect which spreading codes are used by the different data channels of BS k. In other words, we have to detect the index set $\mathcal{D}_k$ of the data channels transmitted by the strongest BS.

A symbol-level model for the received signal in terms of the data channels of the strongest BS is

$$\boldsymbol{x}(u) = \sum_{l \in \mathcal{D}_k} a_k^{(l)} d_k^{(l)}(u)\, \boldsymbol{g}_k^{(l)} + \boldsymbol{w}_k(u), \qquad u = 1, \ldots, U. \tag{14}$$

Here, $\boldsymbol{x}(u)$ is an MQ-dimensional received vector associated to symbol time u; $a_k^{(l)}$ is the amplitude of the lth data channel; $d_k^{(l)}(u)$ is the QPSK symbol of the lth data channel at symbol time u; $\boldsymbol{g}_k^{(l)}$ contains the channel impulse response convolved with the product of the scrambling code of BS k and the spreading code of the lth data channel and truncated to length $Q = 16$; and $\boldsymbol{w}_k(u)$ accounts for the BCH, contributions of weaker BSs, interference from neighboring CDMA symbols, and noise. For simplicity, we model $\boldsymbol{w}_k(u)$ as uncorrelated, white, and complex Gaussian.

When detecting the presence of the data channels in (14), every possible set of data channels corresponds to a distinct hypothesis. Since there are up to 12 parallel data channels in a timeslot, we have $2^{12} = 4096$ different hypotheses; furthermore, the $U = 122$ transmit symbols $d_k^{(l)}(u)$ per data channel act as nuisance parameters. Clearly, the resulting composite hypothesis test would have excessive complexity. To derive a suboptimum detector with moderate complexity, we assume that the vectors $\boldsymbol{g}_k^{(l)}$ for different $l \in \mathcal{D}_k$ are orthogonal so that the presence of each data channel can be detected individually rather than jointly. For each of the 12 possible data channels, we now have a *binary* hypothesis test (data channel present or not). A simple detection statistic for the binary hypothesis test corresponding to the lth data channel is the *incoherent matched filter* [16, p. 158]

$$\Lambda_k^{(l)} = \sum_{u=1}^{U} \left| \boldsymbol{x}^H(u)\, \boldsymbol{g}_k^{(l)} \right|^2.$$

The detected index set $\hat{\mathcal{D}}_k$ is then defined as the set of indices l for which $\Lambda_k^{(l)}$ exceeds a certain threshold. We note that the incoherent matched filter is suboptimum because the distribution of the unknown QPSK transmit symbols $d_k^{(l)}(u)$ in (14) is not circularly symmetric [3], [16]. However, our current task being to detect the presence of a data channel and not the data itself, the actual data can be viewed as nuisance parameters, and a good detector should be as invariant as possible to them. The incoherent matched filter comes close to this goal by ignoring the phase of the QPSK data symbols.

2) Estimation of $\boldsymbol{A}_k$: Having estimated $\boldsymbol{G}_k$ via the detected data channel index set $\hat{\mathcal{D}}_k$ as discussed earlier, it remains to estimate the diagonal amplitude matrix $\boldsymbol{A}_k$ containing the amplitudes $a_k^{(l)}$ for all $l \in \hat{\mathcal{D}}_k$. It can be shown that under ideal conditions (only one BS, no noise, no intersymbol interference), $a_k^{(l)}$ equals a suitably normalized version of $\Lambda_k^{(l)}$. Therefore, we propose to initially use this normalized version of $\Lambda_k^{(l)}$ as an estimate of $a_k^{(l)}$ for detecting $\boldsymbol{d}_k$ according to (12). For the subsequent subtraction/cancellation step, however, a more accurate amplitude estimate should be used. Indeed, once that $\hat{\boldsymbol{d}}_k$ and $\hat{\boldsymbol{G}}_k$ are available, we can compute the least-squares estimate of $\boldsymbol{A}_k$

$$\hat{\boldsymbol{A}}_{k,\mathrm{LS}} \;=\; \arg \min_{\boldsymbol{A}\,\mathrm{diag.}} \|\boldsymbol{x} - \hat{\boldsymbol{G}}_k \boldsymbol{A}\, \hat{\boldsymbol{d}}_k\|^2.$$

This can equivalently be written as $\hat{\boldsymbol{a}}_{k,\mathrm{LS}} = \arg\min_{\boldsymbol{a}} \|\boldsymbol{x} - \hat{\boldsymbol{G}}_k \hat{\boldsymbol{D}}_k \boldsymbol{a}\|^2$, where $\boldsymbol{a}$ is the $13{\cdot}U$-dimensional vector corresponding to the diagonal matrix $\boldsymbol{A}$, and $\hat{\boldsymbol{D}}_k$ is the diagonal $13 \cdot U \times 13 \cdot U$ matrix corresponding to the vector $\hat{\boldsymbol{d}}_k$ (note that $\boldsymbol{A}\hat{\boldsymbol{d}}_k = \hat{\boldsymbol{D}}_k \boldsymbol{a}$). We then obtain [19, p. 225], [20, p. 365]

$$\hat{\boldsymbol{a}}_{k,\mathrm{LS}} \;=\; \hat{\boldsymbol{D}}_k^{-1} \big(\hat{\boldsymbol{G}}_k^H \hat{\boldsymbol{G}}_k\big)^{-1} \hat{\boldsymbol{G}}_k^H \boldsymbol{x}.$$

We now possess estimates of $\boldsymbol{G}_k$, $\boldsymbol{A}_k$, and $\sigma^2_{\boldsymbol{w}_k}$, and thus, we are finally able to calculate an estimate of the correlation matrix $\boldsymbol{R}_{\boldsymbol{x}}$ according to (13).

C. DFB Detector

Following [10], we next develop a DFB modification of the space–time MMSE equalizer (12) that has improved performance [3], [15]. Inserting the estimates $\hat{\boldsymbol{A}}_k$, $\hat{\boldsymbol{G}}_k$, and $\hat{\boldsymbol{R}}_{\boldsymbol{x}}$ derived earlier into (12), we obtain an estimate of the MMSE equalizer matrix $\boldsymbol{F}_{k,\mathrm{MMSE}}$ as

$$\begin{aligned}\hat{\boldsymbol{F}}_{k,\mathrm{MMSE}} &= \hat{\boldsymbol{A}}_k^H \hat{\boldsymbol{G}}_k^H\, \hat{\boldsymbol{R}}_{\boldsymbol{x}}^{-1} \\ &= \hat{\boldsymbol{A}}_k^H \hat{\boldsymbol{G}}_k^H \left(\hat{\boldsymbol{G}}_k \hat{\boldsymbol{A}}_k \hat{\boldsymbol{A}}_k^H \hat{\boldsymbol{G}}_k^H \;+ \widehat{\sigma^2_{\boldsymbol{w}_k}}\, \boldsymbol{I}\right)^{-1}.\end{aligned}$$

The matrix inversion lemma [22, p. 50] yields $\hat{\boldsymbol{F}}_{k,\mathrm{MMSE}} = (\hat{\boldsymbol{A}}_k^H \hat{\boldsymbol{G}}_k^H \hat{\boldsymbol{G}}_k \hat{\boldsymbol{A}}_k + \widehat{\sigma^2_{\boldsymbol{w}_k}}\, \boldsymbol{I})^{-1} \hat{\boldsymbol{A}}_k^H \hat{\boldsymbol{G}}_k^H$. We next use the Cholesky factorization [22, p. 143] $\hat{\boldsymbol{A}}_k^H \hat{\boldsymbol{G}}_k^H \hat{\boldsymbol{G}}_k \hat{\boldsymbol{A}}_k + \widehat{\sigma^2_{\boldsymbol{w}_k}}\, \boldsymbol{I} = \boldsymbol{U}^H \boldsymbol{U}$, where $\boldsymbol{U}$ is a $13 \cdot U \times 13 \cdot U$ upper-triangular matrix. Finally, we define $\tilde{\boldsymbol{U}} \stackrel{\triangle}{=} \mathrm{diag}\{\boldsymbol{U}\}^{-1} \boldsymbol{U}$, where $\mathrm{diag}\{\boldsymbol{U}\}$ is the diagonal matrix with the same diagonal as $\boldsymbol{U}$. We note that $\tilde{\boldsymbol{U}}$ corresponds to a monic filter because its diagonal elements are all equal to 1. The equalized vector (of dimension $13 \cdot U$) can now be written as

$$\boldsymbol{y}_k \;=\; \hat{\boldsymbol{F}}_{k,\mathrm{MMSE}}\, \boldsymbol{x} \;=\; \tilde{\boldsymbol{U}}^{-1} \mathrm{diag}\{\boldsymbol{U}\}^{-2}\, \tilde{\boldsymbol{U}}^{-H}\, \hat{\boldsymbol{A}}_k^H \hat{\boldsymbol{G}}_k^H\, \boldsymbol{x}.$$

Multiplying this equation by $\tilde{\boldsymbol{U}}$ and rearranging the terms, we obtain [10]

$$\boldsymbol{y}_k \;=\; \mathrm{diag}\{\boldsymbol{U}\}^{-2}\, \tilde{\boldsymbol{U}}^{-H}\, \hat{\boldsymbol{A}}_k^H \hat{\boldsymbol{G}}_k^H\, \boldsymbol{x} \;-\; (\tilde{\boldsymbol{U}} - \boldsymbol{I})\, \boldsymbol{y}_k. \qquad (15)$$

Let $y_j \stackrel{\triangle}{=} (\boldsymbol{y}_k)_j$. Since $\tilde{\boldsymbol{U}} - \boldsymbol{I}$ is strictly upper triangular, y_j on the left-hand side of (15) only depends on $y_{j+1}, \ldots, y_J$ on the right-hand side, with $J \stackrel{\triangle}{=} 13 \cdot U$. This allows a recursive calculation of $\boldsymbol{y}_k$. The recursion is initialized with y_J, which can be computed from $\boldsymbol{x}$, $\boldsymbol{U}$, $\hat{\boldsymbol{A}}_k$, and $\hat{\boldsymbol{G}}_k$ alone.

This recursive procedure is still equivalent to the original space–time equalization using $\hat{\boldsymbol{F}}_{k,\mathrm{MMSE}}$. The DFB equalizer is finally obtained by using *quantized versions* $\mathrm{Q}\{y_{j+1}\}, \ldots, \mathrm{Q}\{y_J\}$ of the previously computed components to calculate y_j in every recursion step [10]. That is, (15) is replaced by

$$\boldsymbol{y}_k \;=\; \mathrm{diag}\{\boldsymbol{U}\}^{-2}\, \tilde{\boldsymbol{U}}^{-H}\, \hat{\boldsymbol{A}}_k^H \hat{\boldsymbol{G}}_k^H\, \boldsymbol{x} \;-\; (\tilde{\boldsymbol{U}} - \boldsymbol{I})\, \mathrm{Q}\{\boldsymbol{y}_k\}.$$

V. Simulations

To assess the performance of the proposed receiver algorithms, we conducted Monte Carlo simulations for both a pedestrian environment and an indoor environment.

A. Simulation Setup

Assuming K BSs and channels with P propagation paths (taps) each, the received baseband signal vector $\boldsymbol{x}(n)$ of size $M \times 1$ is given by

$$\boldsymbol{x}(n) \;=\; \sum_{k=1}^{K} \sum_{p=0}^{P-1} \boldsymbol{h}_{k,p}\, s_k(n-p) \;+\; \boldsymbol{n}(n)$$

where $s_k(n)$ is the signal transmitted by the kth BS without power control, $\boldsymbol{h}_{k,p}$ is the $M \times 1$ channel weight vector associated to the kth BS and the pth path, and $\boldsymbol{n}(n)$ is a noise vector. In our simulations, the channel weight vectors were randomly generated using Clarke's channel model [23] $\boldsymbol{h}_{k,p} = \alpha_{k,p} \sum_{q=1}^{N_{k,p}} b_{k,p}^{(q)}\, \boldsymbol{v}_{k,p}^{(q)}$. Here, $\alpha_{k,p}$ is the amplitude of the pth path, $N_{k,p}$ is the number of subpaths of the pth path, the $b_{k,p}^{(q)}$ are independent identically distributed Rayleigh subpath weights, and the $\boldsymbol{v}_{k,p}^{(q)}$ are steering vectors that are determined by the array geometry and the incidence angles. The channel taps $\boldsymbol{h}_{k,p}$ are constant during one timeslot ($666.67\,\mu$s) but change between timeslots; specifically, the coefficients $b_{k,p}^{(q)}$ vary according to a Jakes Doppler spectrum [24, p. 21] corresponding to a mobile velocity of 5 km/h.

The receiver is located in the inner cell of a grid of eight hexagonal cells (see Fig. 8). Thus, we receive one dominant BS signal and seven weaker BS signals. We considered two propagation environments called "pedestrian" and "indoor," with cell radii of 270 m and 30 m, respectively [25]. In addition, we used two different channel parameter settings called A and B. Channel A has three taps with a maximum delay of only 2 chips for both environments, whereas channel B has eight taps with a maximum delay of 15 chips for the pedestrian environment and four taps with a maximum delay of 3 chips for the indoor environment.

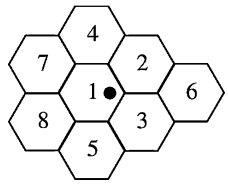

Fig. 8. Simulation scenario. The bullet • indicates the receiver position.

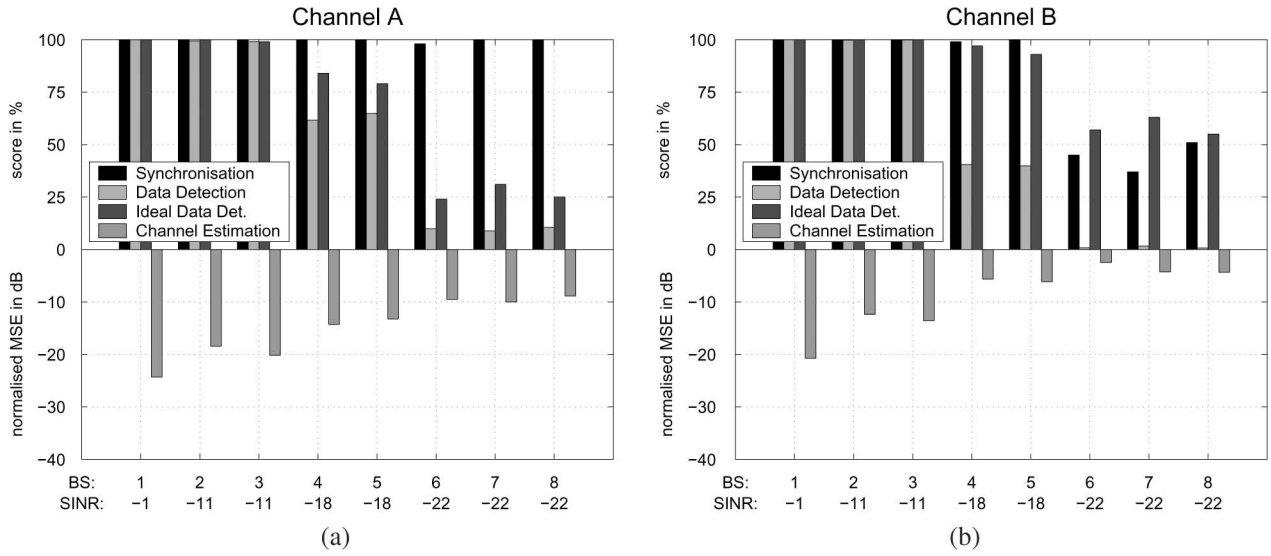

Fig. 9. System simulation results for the pedestrian environment. (a) Channel A. (b) Channel B.

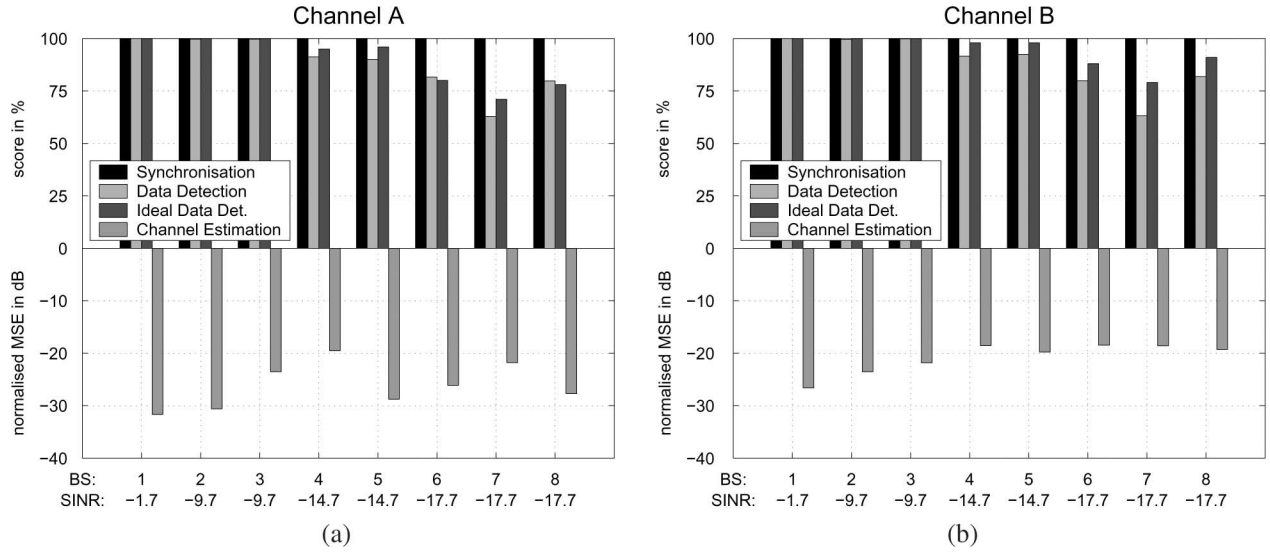

Fig. 10. System simulation results for the indoor environment. (a) Channel A. (b) Channel B.

For an assessment of overall receiver performance, we conducted joint simulations of all three receiver stages. To improve the timing resolution, the sampling rate was chosen as twice the chip rate. We employed the heuristic space–time detector for synchronization, the SC-MMSE estimator for channel estimation, and the SC-DFB detector for data detection. The thresholds for primary synchronization, synchronization verification, and detection of the midamble set (cf. Section III-B) were chosen to obtain a false-alarm probability of 1%, 0.1%, and 1%, respectively. Each of the 100 simulation rounds consisted of 16 frames of data, which were used for averaging the synchronization detection statistic. After channel estimation, we subtracted the SCHs of all BSs detected by the synchronization stage to avoid their detrimental effect on the interference cancellation performance of the subsequent SC-DFB detector. The actual number of channel taps was not known to the receiver, only the maximum channel length L was known.

B. Simulation Results

Figs. 9 and 10 depict the results of our simulations versus the SINR (in decibels) of the different BSs. The graphs show four bars per BS. The first three bars represent the synchronization score (i.e., percentage of successful synchronization events), the BCH data detection score, and for comparison, the hypothetical BCH data detection score obtained with ideal (perfect) synchronization and channel estimation. The fourth bar represents the normalized MSE of the channel estimation stage averaged over all timeslots where the corresponding BS was detected by the synchronization stage.

1) Pedestrian Environment: Looking at Fig. 9, we see that the synchronization results for the pedestrian environment are nearly perfect for channel A and for all but the weakest BSs for channel B. For the weakest BSs for the more hostile channel B, however, the synchronization score drops to about 40%.

The SC-MMSE channel estimator performs quite accurately for channel A, where an MSE of about -10 dB is obtained even for the weakest BSs with an SINR of -22 dB. For channel B, on the other hand, the channel estimation MSE is about -4 dB for BSs with an SINR of -18 and -22 dB. This is because channel B has more taps and is, thus, harder to estimate than the shorter channel A.

For channel A, the *ideal* data detection score of the SC-DFB detector (i.e., assuming perfect synchronization and channel estimation) is above 80% down to SINR $= -18$ dB. It is even better for the longer channel B, due to the increased diversity. The *real* detection performance (with imperfect synchronization and channel estimation) is similar to the ideal case down to SINR $= -11$ dB. At -18 dB, however, the detection score for channel A is reduced from about 80% (ideal case) to about 60%, even though the channel estimation MSE is relatively small (about -13 dB). For the weakest BSs with SINR $= -22$ dB, a similar loss occurs: the detection score drops from about 30% to about 10%, the channel estimation MSE being about -10 dB. For channel B, for a weak BS with SINR $= -18$ dB, the detection score even decreases by 55% from about 95% to 40%. This can be explained by the poor channel estimation results (the channel estimation MSE is about -6 dB). For the weakest BS with SINR $= -22$ dB, where channel estimation accuracy has dropped to an MSE of -4 dB, detection is virtually impossible.

2) Indoor Environment: In the indoor environment (see Fig. 10), the synchronization stage works perfectly: a score of 100% is achieved for all BSs. Also, the channel estimation is quite accurate. For channel A, the channel estimation MSE is well below -20 dB for practically all BSs. For channel B, the MSE is a little higher, but the worst value of -18 dB is still very low. The *ideal* detection score is over 80% down to SINR $= -17.7$ dB. The detection performance is only a little better for channel B, because channel B is just one tap longer than channel A, and thus, the gain in diversity is small. Due to the good performance of the synchronization and channel estimation stages (which can be explained by the smaller number of channel taps for the indoor environment compared to the pedestrian environment), the *real* detection performance of the overall system is nearly equal to the ideal case. Only for the weakest BSs (SINR $= -17.7$ dB), the detection score drops by 10%, but it is still around 70%.

VI. Conclusion

We presented receiver signal processing techniques for a network monitoring device that analyzes the interference in a UMTS/TDD system. The widely differing power levels of the signals received from different BSs called for advanced multiuser space–time algorithms for synchronization, channel estimation, and data detection. To meet the challenges posed by the large power differences and the partial lack of relevant prior knowledge, we modified and combined sophisticated estimation and detection techniques, e.g., by embedding them in reestimation and successive cancellation schemes.

Our simulations demonstrated good performance of the presented algorithms in the difficult real-world scenario considered. Specifically, the synchronization stage almost always performed satisfactorily. The channel estimation was very accurate for the indoor environment and the strongest BSs in the pedestrian environment, but much less so for the weaker BSs in the pedestrian environment. This may be explained by the poor accuracy of the least-squares channel estimates in these cases, which causes the resulting estimates of the channel statistics to be inaccurate too. Finally, we observed that for satisfactory performance of data detection, a channel estimation MSE of $-20 \ldots -16$ dB is needed; with an MSE of -10 dB, the detection score must be expected to be reduced by about 20%. We also observed that the diversity advantage of longer channels is reduced by larger channel estimation errors.

Acknowledgment

The authors would like to thank P. Loubaton and J.-M. Chaufray for helpful discussions. They are also grateful to the reviewers for their comments that have resulted in a clearer presentation.

References

[1] K. Kopsa, G. Matz, H. Artés, and F. Hlawatsch, "Space–time synchronization algorithms for UMTS/TDD systems with strong co-channel interference," in *Proc. IEEE Globecom 2002*, Taipei, Taiwan, Nov. 2002, pp. 254–258.

[2] K. Kopsa, H. Artés, G. Matz, and F. Hlawatsch, "Space–time algorithms for multiuser channel estimation in the downlink of UMTS/TDD," in *Proc. IEEE ICC 2003*, Anchorage, AK, May 2003, pp. 2406–2410.

[3] H. Artés, K. Kopsa, and F. Hlawatsch, "A multi-antenna detection algorithm for UMTS/TDD receivers in strong interference environments," in *Proc. IEEE Globecom 2003*, San Francisco, CA, Dec. 2003, pp. 819–823.

[4] http://www.umts-forum.org

[5] http://cordis.europa.eu/data/PROJ_FP5/ACTIONeqDndSESSIONeq112422005919ndDOCeq177ndTBLeqEN_PROJ.htm

[6] D. Depierre, F. Pipon, P. Loubaton, and J.-M. Chaufray, "Multi-sensor synchronization and demodulation algorithms in the downlink of the UMTS FDD mode," in *Proc. COST 273 Workshop Broadband Wireless Local Access*, Paris, France, May 2003.

[7] A. Naguib and A. Paulraj, "Performance of CDMA cellular networks with base-station antenna arrays," in *Proc. Int. Zürich Seminar Digit. Commun.*, Zürich, Switzerland, Mar. 1994, pp. 87–100.

[8] J. S. Thompson, P. M. Grant, and B. Mulgrew, "Smart antenna arrays for CDMA systems," *IEEE Pers. Commun.*, vol. 3, no. 5, pp. 16–25, Oct. 1996.

[9] S. Miller and S. Schwartz, "Integrated spatial-temporal detectors for asynchronous Gaussian multiple access channels," *IEEE Trans. Veh. Technol.*, vol. VT-40, pp. 472–482, May 1995.

[10] A. Klein, G. K. Kaleh, and P. W. Baier, "Zero forcing and minimum mean square error equalization for multiuser detection in code-division multiple-access channels," *IEEE Trans. Veh. Technol.*, vol. 45, no. 2, pp. 276–287, May 1996.

[11] A. Paulraj and C. B. Papadias, "Space–time processing for wireless communications," *IEEE Signal Process. Mag.*, vol. 14, no. 6, pp. 49–83, Nov. 1997.

[12] P. van Rooyen, M. Lötter, and D. van Wyk, *Space–Time Processing for CDMA Mobile Communications*. Norwell, MA: Kluwer, 2000.

[13] 3GPP. (2001 Mar.). TS 25.221 Physical channels and mapping of transport channels onto physical channels (TDD) TS 25.221 v. 4.0.0 [Online]. Available: www.3gpp.org.

[14] 3GPP. (2001 Mar.). TS 25.223 Spreading and modulation (TDD) TS 25.223 v. 4.0.0 [Online]. Available: www.3gpp.org.

[15] K. Kopsa, "Space–time processing for UMTS/TDD," Ph.D. dissertation, Vienna Univ. Technol., Vienna, Austria, Sep. 2007.
[16] S. M. Kay, *Fundamentals of Statistical Signal Processing: Detection Theory*. Upper Saddle River, NJ: Prentice-Hall, 1998.
[17] L. E. Brennan and I. S. Reed, "An adaptive array signal processing algorithm for communications," *IEEE Trans. Aerosp. Electron. Syst.*, vol. 18, no. 1, pp. 124–130, Jan. 1982.
[18] D. M. Dlugos and R. A. Scholtz, "Acquisition of spread spectrum signals by an adaptive array," *IEEE Trans. Acoust., Speech, Signal Process.*, vol. 37, no. 8, pp. 1253–1270, Aug. 1989.
[19] S. M. Kay, *Fundamentals of Statistical Signal Processing: Estimation Theory*. Englewood Cliffs, NJ: Prentice-Hall, 1993.
[20] L. L. Scharf, *Statistical Signal Processing*. Reading, MA: Addison Wesley, 1991.
[21] P. A. Bello, "Characterization of randomly time-variant linear channels," *IEEE Trans. Commun. Syst.*, vol. 11, no. 4, pp. 360–393, Dec. 1963.
[22] G. H. Golub and C. F. Van Loan, *Matrix Computations*, 3rd ed. Baltimore, MD: Johns Hopkins Univ. Press, 1996.
[23] R. H. Clarke, "A statistical theory of radiomobile reception," *Bell Syst. Tech. J.*, vol. 47, pp. 957–1000, 1968.
[24] W. C. Jakes, *Microwave Mobile Communications*. New York: Wiley, 1974.
[25] ETSI, "Selection procedures for the choice of radio transmission technologies for the UMTS," Tech. Rep. TR 101.112, Apr. 1998.

Klaus Kopsa received the Dipl.-Ing. and Dr. Techn. degrees in electrical engineering from Vienna University of Technology, Vienna, Austria, in 1998 and 2003, respectively.

From 1998 to 2003, he was with the Institute of Communications and Radio Frequency Engineering, Vienna University of Technology, where he focused on space–time signal processing for third generation mobile communications systems. Since 2004, he has been with Accenture, Vienna, participating mainly in systems-integration projects in the communications industry.

Harold Artés (S'98–M'05) received the Dipl.-Ing. and Ph.D. degrees in electrical engineering from Vienna University of Technology, Vienna, Austria, in 1997 and 2003, respectively.

From December 1997 to February 2004, he was a Research (and partly Teaching) Assistant with the Institute of Communications and Radio-Frequency Engineering, Vienna University of Technology. From April 2004 to April 2005, he was a Postdoctoral Fellow with Stanford University, Stanford, CA. He then joined Beceem Communications, Santa Clara, CA, where he is currently heading the algorithm development for WiMax OFDMA subscriber stations. His research interests include multiple-input multiple-output wireless communications, multiuser techniques, and statistical signal processing in general. He has coauthored two patents.

Dr. Artés participated in the European Commission's IST Project ANTIUM.

Gerald Matz (S'95–M'01–SM'07) received the Dipl.-Ing. and Dr. Techn. degrees in electrical engineering and the Habilitation degree for communication systems from Vienna University of Technology, Vienna, Austria, in 1994, 2000, and 2004, respectively.

Since 1995, he has been with the Department of Communications and Radio-Frequency Engineering, Vienna University of Technology, where he currently holds a tenured position as an Associate Professor. From March 2004 to February 2005, he was on leave as an Erwin Schrödinger Fellow with the Laboratoire des Signaux et Systèmes, Ecole Supérieure d'Electricité, Gif-sur-Yvette, France. His research interests include wireless communications, statistical signal processing, and information theory. He has authored more than 90 publications in international journals, conference proceedings, and edited books.

Prof. Matz has directed or actively participated in several research projects funded by the Austrian Science Fund and by the European Union. He is an Associate Editor of the IEEE TRANSACTIONS ON SIGNAL PROCESSING and the IEEE SIGNAL PROCESSING LETTERS. He was Technical Program Co-Chair of the 12th European Signal Processing Conference and a member of the program committees of numerous IEEE conferences. In 2006, he received the Kardinal Innitzer Most Promising Young Investigator Award.

Franz Hlawatsch (S'85–M'88–SM'00) received the Diplom-Ingenieur, Dr. Techn., and Univ.-Dozent (habilitation) degrees in electrical engineering/signal processing from Vienna University of Technology, Vienna, Austria, in 1983, 1988, and 1996, respectively.

Since 1983, he has been with the Institute of Communications and Radio-Frequency Engineering, Vienna University of Technology, where he currently holds an Associate Professor position. From 1991 to 1992, as a recipient of an Erwin Schrödinger Fellowship, he spent a sabbatical year with the Department of Electrical Engineering, University of Rhode Island, Kingston, RI. In 1999, 2000, and 2001, he held one-month Visiting Professor positions with INP/ENSEEIHT/TeSA, Toulouse, France and IRCCyN, Nantes, France. He (co)authored a book, about 160 refereed scientific papers and book chapters, and two patents, and coedited two books. His research interests include signal processing for wireless communications, nonstationary statistical signal processing, and time–frequency signal processing.

Prof. Hlawatsch was Technical Program Co-Chair of the 12th European Signal Processing Conference (EUSIPCO 2004) and served on the technical committees of numerous IEEE conferences. From 2003 to 2007, he was an Associate Editor for the IEEE TRANSACTIONS ON SIGNAL PROCESSING. Since 2004, he has been a member of the IEEE SPCOM Technical Committee. He is coauthor of a paper that won an IEEE Signal Processing Society Young Author Best Paper Award.